

A CFD assessment to Subsonic flow around NACA4412

Ali Abud AL-Nabi Abass
Affairs Contracts Department
The University of Mustansiriya
triplea71@yahoo.com

Abstract

The purpose of this study is determined values of Mach Number (Ma) for Subsonic flow around NACA4412 which is begun shock wave and known the location it. A 2-dimensional triangular C-type grid is used to match the reference measurements at an airfoil cross-section was taken from NACA 4412 from leading edge to trailing edge. The Mach numbers which used are (0.1 to 0.9) respectively and angles of attack (2.31° and 0.0°) for three cases inviscid and viscous flow with choose two cases (K epsilon RNG and Spalart-Allmaras turbulent models).

The numerical results show that the inviscid and two turbulence models well predict the shock wave location and size as well as flow properties along the airfoil surface. The Lift Force Coefficient (CL) decrease and the Drag Force Coefficient (CD) increase with using viscous term as well as pressure coefficient (CP) give fit location for the shock wave

Keyword:

Computational fluid dynamics(CFD), turbulence models, subsonic flow, Spalart-Allmaras Model, k-epsilon rng model, grid technique,

التخمين باستخدام CFD لجريان الهواء دون سرعة الصوت لمقطع جناح NACA 4412

الخلاصة

الغرض من هذه الدراسة تحديد قيم عدد ماخ للجريان تحت الصوتي حول مقطع جناح NACA 4412. الشبكة المستخدمة ثلاثية الخلية ذات بعد ثنائي نوع سي تم استخدام تمثيل التوزيع النقطي لرسم سطح الجناح المقياس السطحي للجناح والذي اخذ من NACA 4412 من نقطة حافة البداية الى النهاية. أعداد ماخ المستخدمة كانت (0.9-0.1) بالترتيب وزايتا هجوم (2.31° و 0.0°) درجة لثلاثة حالات جريان غير لزج وحالتين جريان لزج (K-epsilon RNG and Spalart-Allmaras turbulent models)

النتائج العددية بينت بان الجريان الغير لزج بالإضافة إلى الجريان اللزج بنوعيه أعطى تخمين جيد لموقع الموجة الصدمية وحجمها وكذلك خصائص الجريان على طول سطح الجناح تم ملاحظة انخفاض معامل الرفع مع ازدياد معامل الكبح مع استخدام حدود اللزوجة وكذلك استخدام معامل الضغط أعطى تصور جيد لموقع الصدمة.

Introduction

The design for model of airfoil such as NACA 4412 demanded knowledge aerodynamic properties. It was built by using GAMBIT code, chosen and specified clustering the mesh generation with boundary conditions. To study the flow properties such as Lift Force Coefficient and Drag Force Coefficient, three cases were taken inviscid and viscose flow (by using K epsilon (e) RNG and Spalart-Allmaras turbulent models). This study is limited the effect of shock wave on flow properties for flow on airfoil surface by using the curves of lift and drag force coefficients and curves of pressure coefficient on the wall while is showed the size and location of shock waves through Mach number contours.

Various experimental and theoretical studies have been published about NACA 4412. Omar Badran et al(2003)[1]. studied mean flow and Reynolds stresses results, of a NACA 4412 airfoil, covering the boundary layers around the airfoil and the wake region at angle of attack, $\alpha = 15^\circ$. Two-equation turbulence models are tested on NACA 4412 airfoil at the position of maximum lift (angle of attack = 15°). These models are the two-equation Realizable and RNG k-e models and the Reynolds Stress Model (RSM). It was found that the developed turbulence models had captured the physics of unsteady separated flow. The resulting surface pressure coefficients, skin friction, velocity vectors, and Reynolds stresses are compared with flying hot wire experimental data, and the models produce very similar results. Also excellent agreements between computational and experimental surface pressures and skin friction were observed. Also excellent agreement between computational and experimental surface pressures and skin friction was observed. Serhat Duran(2005)[2]. Modified blade shape by using NACA 4412. The output of the blade design program performed for the airfoil NACA 4412 When the designed blade shape is modified, it is seen that the power extracted from the wind is reduced about 10% and the length of modified blade is increased about 5% for the same required power. Modification of blade geometry promised to be a good approximation would be explained it. B. Greschner et al (2005)[3] investigated unsteady flows around a series of NACA airfoils included NACA 4412 carried out. They designed case studies on the connections between an airfoil shape characteristics and its aerodynamic and aeroacoustic performance, employed the unsteady CFD flow simulations in the near field of an airfoil. The results include identifying the optimum symmetric and asymmetric airfoils among the airfoils and suggesting the possible optimum airfoil characteristics. The results can be used to guide the selections of the geometric parameters and constraints in a fully automated aerodynamic and aeroacoustic optimization. Manish K et al (2005)[4]. Studied CL, CD on NACA 4412 and NACA 0011 at Mach number 0.2 and

different angles of attack (0.0° to 14°) and determined the effect of Gurney flap on NACA 4412 and NACA 0011 airfoils for Two dimensional steady state Navier-Stokes, used to predict the flow field around the airfoils. Gurney flap sizes selected for the study range from 0.5% to 4% of the airfoil chord. They Computed results have been compared with available experimental and computational data. There was good correlation observed between computed and experimental data. Addition of Gurney flap increased the lift coefficient significantly with very little drag penalty if proper Gurney flap height was selected.

Inviscid flow

For studying inviscid flow Euler equation by Ali Al-Hussaini [5]:

Continuity equation:

$$\frac{\partial \rho}{\partial t} + \frac{\partial(\rho u)}{\partial x} + \frac{\partial(\rho v)}{\partial y} = 0 \dots\dots\dots (1)$$

The conservation of momentum equation is:

$$\frac{\partial(\rho u)}{\partial t} + \frac{\partial}{\partial x}(\rho u^2 + p) + \frac{\partial}{\partial y}(\rho uv) = 0 \dots\dots\dots (2)$$

$$\frac{\partial(\rho v)}{\partial t} + \frac{\partial}{\partial x}(\rho uv) + \frac{\partial}{\partial y}(\rho v^2 + p) = 0 \dots\dots\dots (3)$$

The conservation of energy equation is

$$\frac{\partial(E_t)}{\partial t} + \frac{\partial}{\partial x}[(E_t + p)u] + \frac{\partial}{\partial y}[(E_t + p)v] = 0 \dots\dots\dots (4)$$

Where ρ : density (Kg/m³) , u: Velocity component in x direction (m/s), v: Velocity component in y direction (m/s), p: pressure (Pa), E_t: Total internal energy per unit volume (J/m³)

The RNG K-ε Model

Yakhot, et al. [6] have proposed a variant of the k-ε-Model to improve performance characteristics compared to the standard model. The new model is based on the Renormalization-Group-Theory [7], and is referred to as “RNG”-k-ε-Model. The transport equations of the RNG are very similar to the standard (k-ε) model, but employ an additional source/sink term in the (ε) equation and the values of the coefficients differ from those in the standard (k-ε) model. The turbulent kinetic energy, k, and its rate of dissipation, ε epsilon, are obtained from the following transport equations::

$$\rho \frac{Dk}{Dt} = \frac{\partial}{\partial x} \left(\alpha k \mu_{eff} \frac{\partial k}{\partial x} \right) + G + B - \rho \varepsilon - YM \dots\dots\dots(5)$$

And

$$\rho \frac{D\varepsilon}{Dt} = \frac{\partial}{\partial x} \left(\alpha \varepsilon \mu_{eff} \frac{\partial \varepsilon}{\partial x} \right) + C1 \frac{\varepsilon}{k} (G + C_3 B) - C_2^* \rho \frac{\varepsilon^2}{k} \dots\dots\dots(6)$$

Where C1, C2 and C3 are empirical coefficients and σ_k and σ_ε are the turbulent Prandtl number respectively Schmidt number. The effective viscosity μ_{eff} (Equation (5, 6) in Modeling the Effective Viscosity) to account for low-Reynolds-number effects.

$$\mu_{eff} = |\alpha\omega - 1.3929|^{0.6321} |\alpha\omega + 2.3929|^{0.3679} \text{ where } \alpha\omega=1 \text{ in the high Reynolds No.}$$

$$C_2^* = \left(C_2 + \frac{C_\mu \rho \eta^3 (1 - \eta/\eta_0)}{1 + \beta \eta^3} \right) \dots\dots\dots(7)$$

The term B is the buoyancy-term (depending on whether stratification is stable or unstable) ($B \approx \frac{\mu_t}{\rho \sigma_p} \rho g$). Where B: depends on the fluctuating density field, where σ_p is the turbulent Prandtl / Schmidt number for density.

The dilation dissipation term in the k-equation $YM = \rho \varepsilon^2 \sqrt{K/a^2}$ is modelled according to Sarker, a: sound speed [8].

S is the tensor of the mean rate-of-strain, defined as:

$$\text{With } \eta = S \frac{k}{\varepsilon} \text{ and } S = \sqrt{2s_{ij}s_{ij}} = \sqrt{G/\mu_t} \text{ with } s_{ij} = \frac{1}{2} \left(\frac{\partial u_i}{\partial x_j} + \frac{\partial u_j}{\partial x_i} \right). \text{ It can be shown that } \eta \text{ is a}$$

function of generation and dissipation of k and can be Written as $\eta = \sqrt{C_\mu^{-1} \frac{G}{\rho \varepsilon}}$ which indicates that η characterises the equilibrium characteristic of the turbulence field.

$C_\mu = 0.09$, ($G = \mu_t S^2$), $\mu_t = C_\mu \rho \frac{K^2}{\varepsilon}$ the two new coefficients, η_0 and β , can be obtained directly from the primary model coefficients and the Von Karman constant, $\eta_0 = 4.38$ and $\beta = 0.012$. These values are referred to as the ‘‘original’’ set of coefficients. The quantities α_k and α_ε are the inverse effective Prandtl numbers for k and ε .

Yakhot, et al. [6] recommended the following set of model coefficients:

Coef.	σ_k	σ_ε	c_1	c_2	Von-Karman constant	α_k	α_ε
value	0.71	0.71	1.42	1.70	0.39	1.393	1.393

Spalart-Allmaras Model

The Spalart & Allmaras model belongs to the one equation family of eddy viscosity models. This family is based on the assumption that Reynolds stress-tensor $-\rho \cdot \overline{u'v'}$ is related to the mean strain rate through an apparent turbulent viscosity called eddy viscosity ν_t , which can be computed from the Reynolds Stresses:

$$-\overline{u'v'} = \nu_t \cdot \left(\frac{\partial \bar{u}}{\partial y} + \frac{\partial \bar{v}}{\partial x} \right)$$

Actually the computation uses an intermediate transport variable $\tilde{\nu}$ with the damping function $f_{v1}(\chi)$ relating to turbulent viscosity by $\nu_t = \tilde{\nu} f_{v1}(\chi)$ to solve the following transport equation

$$\rho \frac{D\tilde{\nu}}{Dt} G_v + \frac{1}{\sigma_{\tilde{\nu}}} \left[\frac{\partial}{\partial x_j} \left\{ (\mu + \rho \cdot \tilde{\nu}) \cdot \frac{\partial \tilde{\nu}}{\partial x_j} \right\} + C_{b2} \cdot \rho \left(\frac{\partial \tilde{\nu}}{\partial x_j} \right)^2 \right] - Y_v \dots \dots \dots (8)$$

The intermediate variable $\tilde{\nu}$ is in general identical to the turbulent kinematic viscosity ν_t except in the near-wall region [9].

G_v and Y_v are the production and destruction terms of turbulent viscosity. Both are strong in the near-wall region due to wall blocking and viscous damping. Besides $\sigma_{\tilde{\nu}}$ denotes the turbulent Prandtl number, C_{b2} a calibration constant and ν is the molecular kinematic viscosity.

Boundary conditions specify the flow and properties variables on the boundaries of the physical model. The boundary conditions in GAMBIT are classified, flow inlet and exit boundaries: pressure far field, pressure outlet, Wall, the internal face boundary conditions are defined on cell faces, which means that they do not have a finite thickness and they provide a means of introducing a step change in flow properties[10].

In solid wall, there are two types of flow on the wall, depending on viscous or inviscid flow, wherein viscous wall boundary condition, no-slip condition, enforced at walls, tangential fluid velocity equal to wall velocity. Normal velocity component = 0, shear stress can also be specified [10].

In inviscid wall boundary condition imposes flow tangency at the zone boundary (wall surface) while maintaining the same total velocity as the point adjacent to the boundary [10].

The far field boundary conditions are more difficult to specify in a way that facilitates computation. It is necessary to differentiate between inflow and outflow boundary conditions, which can determine pressure far field, pressure outlet boundary condition.

Pressure outlet boundary conditions are used to define the static pressure at flow outlet. The use of a pressure outlet boundary condition instead of an outflow condition often results in a better rate of convergence when backflow occurs during iteration .

Pressure far field boundary conditions are used to model a free stream compressible or incompressible flow at infinity, with free stream Mach number and static conditions specified. For grid generation FLUENT used grids comprising of triangular. the major motivation for using unstructured grids employing triangular cells, the range of length scales of the flow is large, a triangular mesh can often be created with far fewer cells than the equivalent mesh consisting of quadrilateral cells. This is because a triangular mesh allows cells to be clustered in selected regions of the flow domain, whereas structured quadrilateral meshes will generally force cells to be placed in regions where they are not needed, the reason behind case in the current study unstructured triangular meshes as shown fig (1) [4].

At convergence, all discrete conservation equations (momentum, energy, etc.) obey in all cells to a specify tolerance. Solution no longer changes with more iteration, solution to equation on overall mass, momentum, energy, and scalar balances are obtained. Monitoring convergence with residuals, generally shows, a decrease in residuals by 3 orders of magnitude indicating at least qualitative convergence, major flow features established, scaled species residual may need to decrease to 10^{-4} to achieve species balance, monitoring quantitative convergence and monitoring other variables for changes, ensure that conservation satisfies the convergence [4].

Results and Discussion

The flow computations required about 800 iterations to converge. At the end of every computational run, flow residuals are reduced by more than three orders of magnitude. An example of residual history is shown in Fig 2.

At angle of attack $=2.31^{\circ}$. The shock wave started creation and separation flow on the surface of trail of airfoil at Mach-number 0.7 and angle of attack $=2.31^{\circ}$ as shown in Figures (3, 3a, 4, 4a and 5a) while the flow is subsonic as shown in fig. 5.

The general effect of Mach number 0.729 and separation flow on the trail of airfoil shown in Figures (6, 6a, 7, 7a, 8, and 8a). Especially the size and location of the shock wave region ($Ma > 1,0$) can be seen at ($X/C > 15$).

The shock wave grew moving towards tail as well as the interaction with the boundary layer after flow separation as shown in figures (9, 9a, 10, 10a, 11 and 11a). At last the location of shock in ($X/C \geq 70$).

At angle of attack $=0.0^{\circ}$, Mach numbers (0.7 and 0.729), the figures (12, 12a, 13, 13a, 14, 14a, 15, 15a, 16, 16a, 17, 17a) in Mach number contours shown location and size shock wave at ($x/c \geq 50$) while velocity magnitude contours appeared the boundary layer on the surface of trail of airfoil.

Figures (18, 18a, 19, 19a, 20, 20a) shown Mach number and velocity magnitude contours the behavior of flow properties are similar to previous cases at Mach number 0.8 .

In Figures (12, 13 and 14) the pressure distribution along airfoil surface is presented by pressure coefficient. The comparison of the chosen turbulence models with inviscid flow

which is one of the main subjects of the investigation. The curves of all three models fit and give a good indication to the location of the shock wave. The high gradient in pressure coefficient ($X/C \approx 15, 17.5$ and 50) indicates the back boundary of the shock region. The effect of the viscosity was gradually increased which cause the deference between the C_D and C_L . when increase the value of Mach number above 0.7 the values of C_L and C_D are jump because of the shock wave was created on the middle surface of airfoil as shown in the figures (15, 16).

Conclusion

As the aim of study the effect of shock wave on airfoil surface is to know the value of Mach number, which start to create shock wave and effect boundary layer on the shock. The calculations show good agreement in values of Mach number 0.729 in three cases on RAE 2822, at angle of attack 2.31° with Al-Dulaimy [11], but it deferent in the location of shock wave because the shape of airfoil for this reason different the results from angle of attack 0.0° . The curves of pressure coefficient give exact location for shock wave. The curves of C_L , C_D and C_P give effect of shock wave on C_L , C_D and C_P on surface of airfoil. The effect of viscosity is clearance on C_L , C_D and values of Mach numbers contours but is disappear in pressure coefficient .

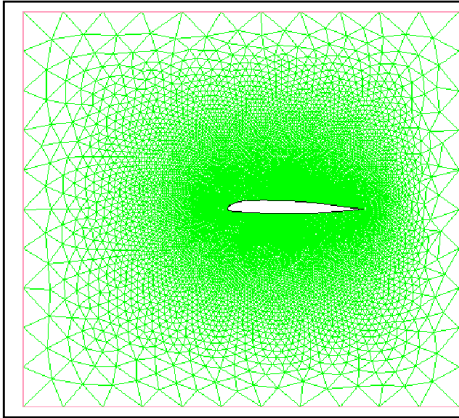


**Fig.1 Grid Generation
(Triangular Mesh, C-Type)**

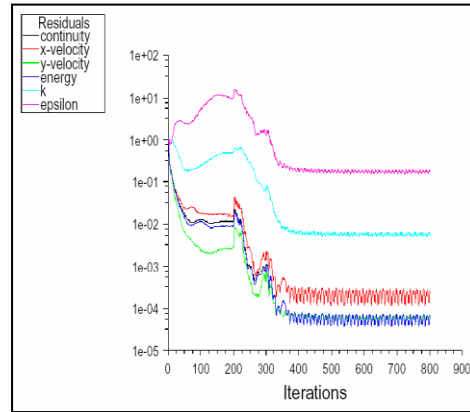


**Fig.2 Residual history of
Solution Convergence**

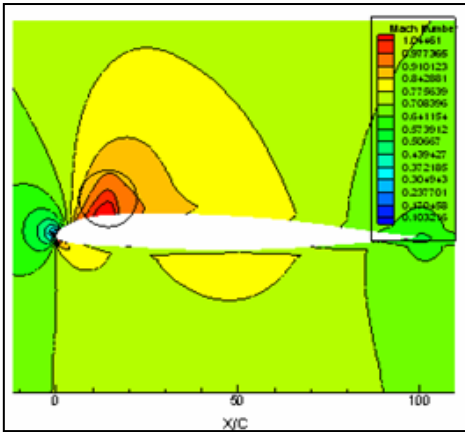


**Fig. 3 Mach number contours
(free stream Mach number 0.7 for
inviscid flow and $\alpha=2.31$ degree)**

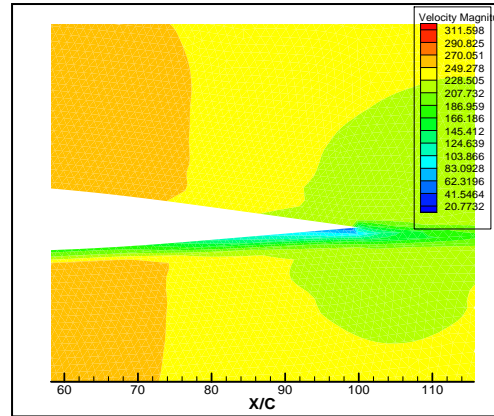


**Fig.3a velocity magnitude contours
At Mach Number 0.7 for inviscid
flow and $\alpha=2.31$ degree**

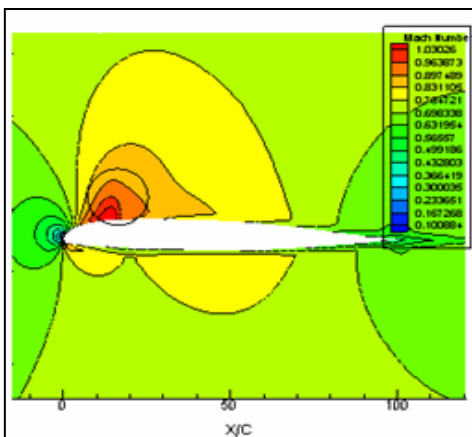


**Fig. 4 Mach number contours
(free stream Mach number 0.7
for k-epsilon RNG flow
and $\alpha=2.31$ degree)**

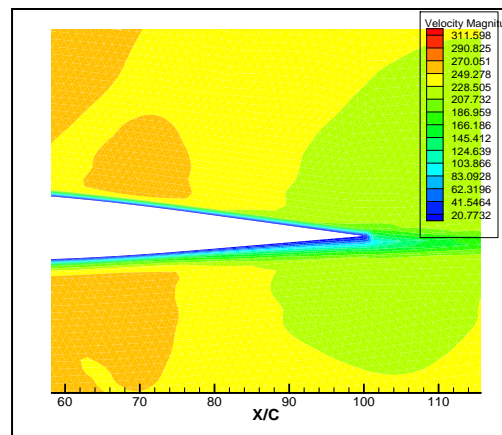


**Fig.4a velocity magnitude
contours at Mach number 0.7
for k-epsilon RNG flow and
 $\alpha=2.31$ degree**

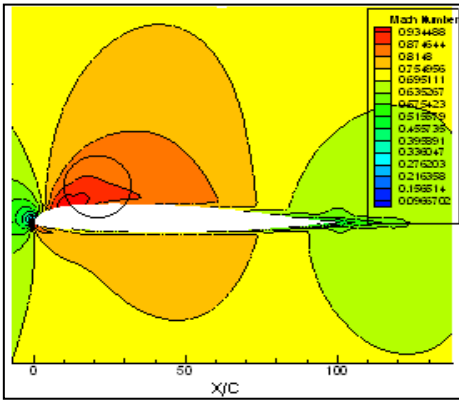


Fig. 5 Mach number contours (free stream Mach number 0.7 for Spalart-Allmaras flow and $\alpha=2.31$ degree

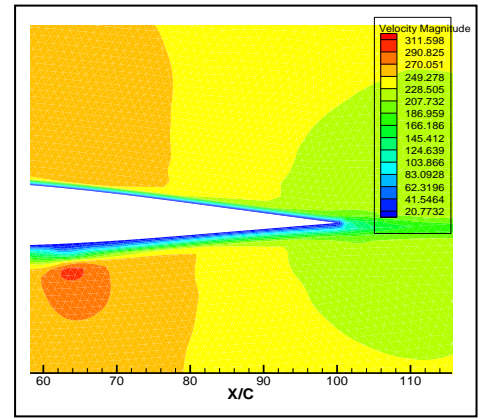


Fig.5a velocity magnitude contours at Mach number 0.7 for Spalart-Allmaras flow and $\alpha=2.31$ degree

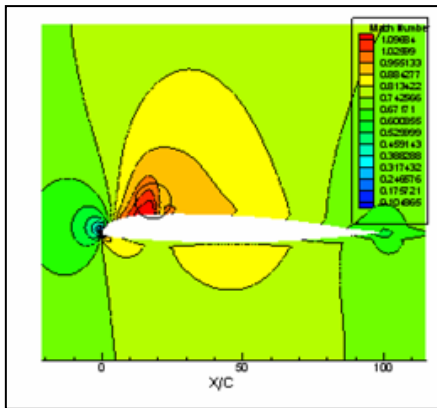


Fig. 6 Mach number contours (free stream Mach number 0.729 for inviscid flow and $\alpha=2.31$ degree)

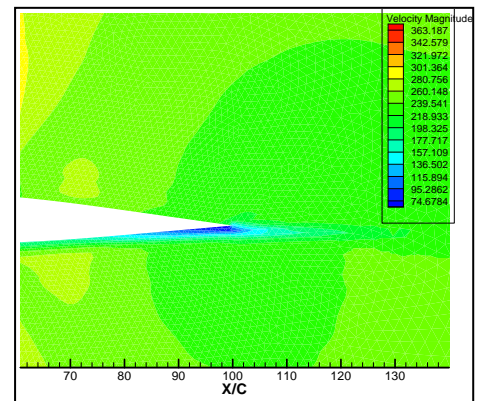


Fig.6a velocity magnitude contours at Mach number 0.729 for inviscid flow and $\alpha=2.31$ degree

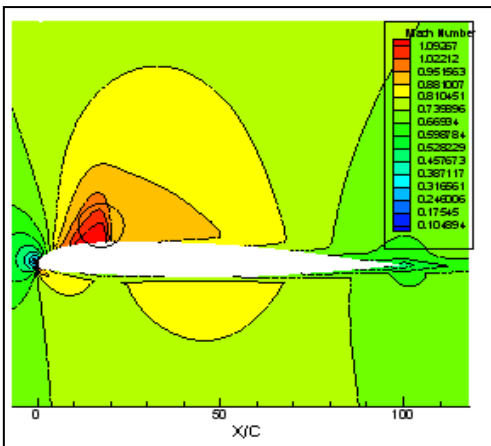


Fig. 7 Mach number contours (free stream Mach number 0.729 for k-epsilon RNG flow and $\alpha=2.31$ degree)

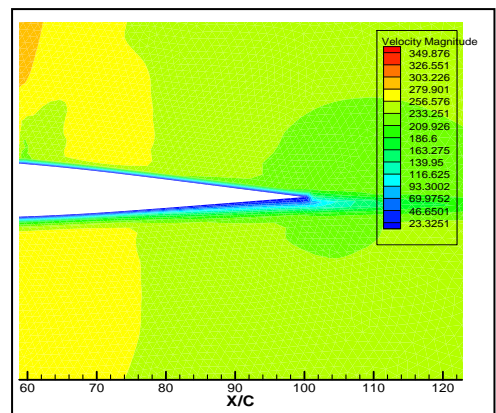


Fig.7a velocity magnitude contours at Mach number 0.729 for k-epsilon RNG flow and $\alpha=2.31$ degree

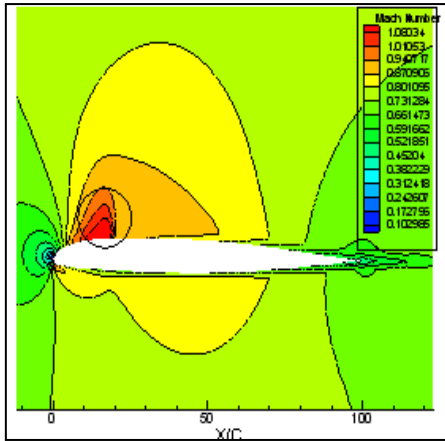


Fig. 8 Mach number contours (free stream Mach number 0.729 for Spalart- Allmaras flow and $\alpha=2.31$ degree)

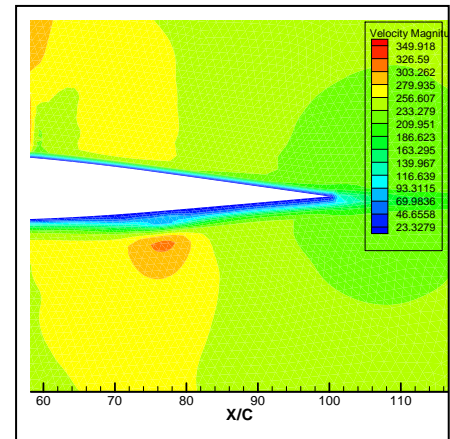


Fig8a velocity magnitude contours at Mach number 0.729 for Spalart Allmaras flow and $\alpha=2.31$ degree

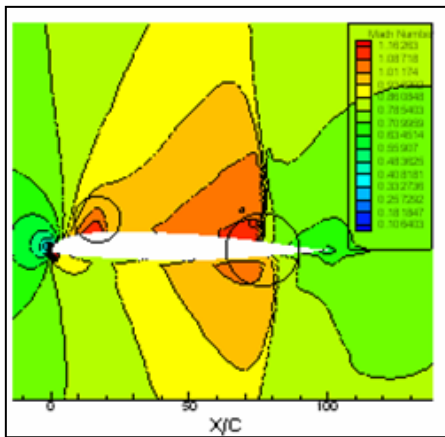


Fig. 9 Mach number contours (free stream Mach number 0.8 for inviscid flow and $\alpha=2.31$ degree)

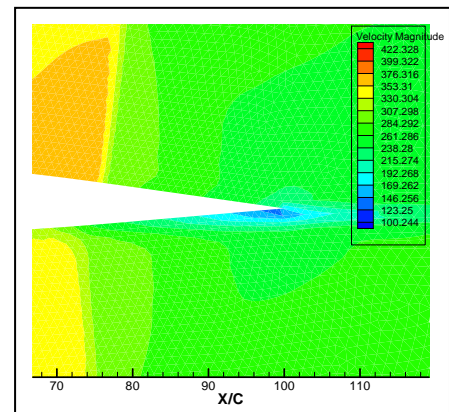


Fig.9a velocity magnitude contours at Mach number 0.8 for inviscid flow and $\alpha=2.31$ degree

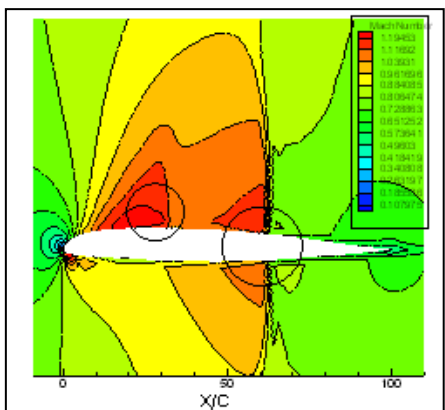


Fig. 10 Mach number contours (free stream Mach number 0.8 for k-epsilon RNG flow and $\alpha=2.31$ degree)

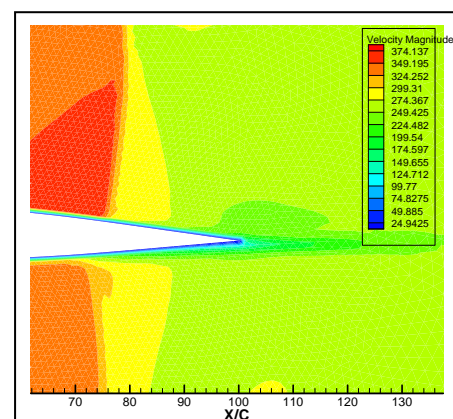


Fig.10a velocity magnitude contours at Mach number 0.8 for k-epsilon RNG flow and $\alpha=2.31$ degree

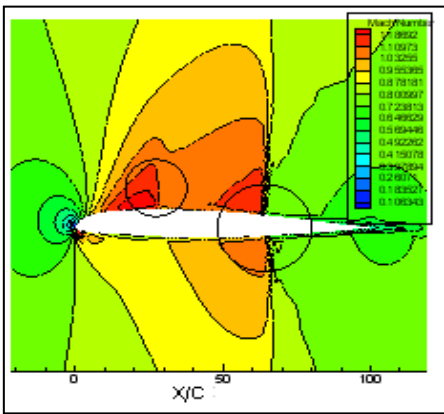


Fig. 11 Mach number contours free stream Much number 0.8 for Spalart- Allmaras flow and $\alpha=2.31$ degree)

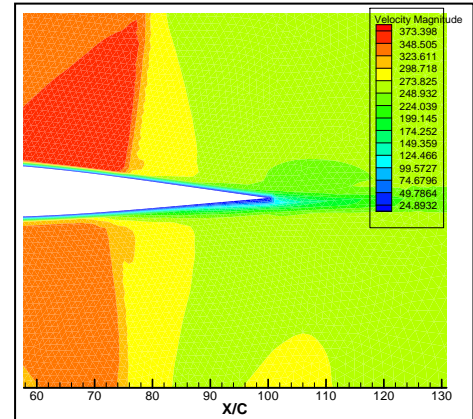


Fig. 11a velocity magnitude contours at Mach number 0.8 for Spalart- Allmaras flow and $\alpha=2.31$ degree

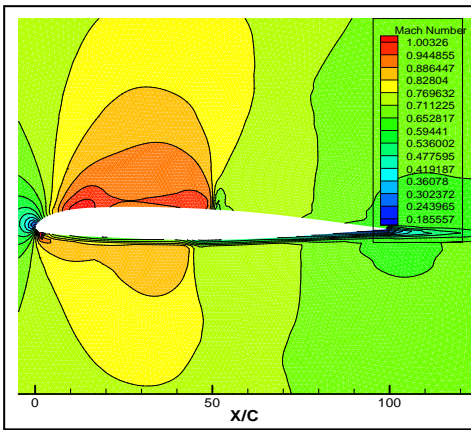


Fig 12 Mach number contours (free stream Mach number 0.7 for inviscid flow and $\alpha=0.0$ degree

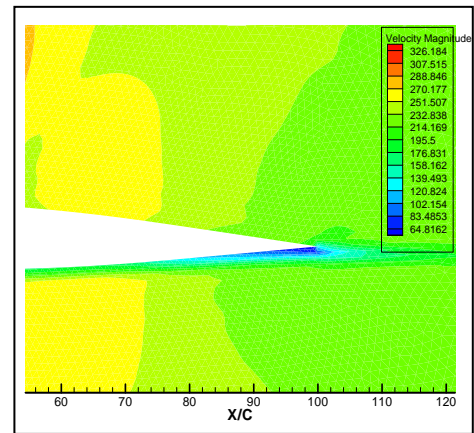


Fig.12a velocity magnitude contours at Mach number 0.7for inviscid flow and) $\alpha=0.0$ degree

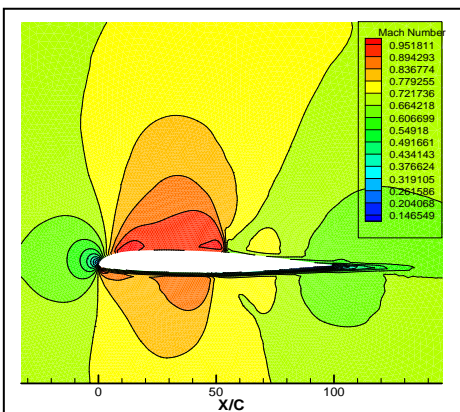


Fig 13 Mach number contours (free stream at Mach number 0.7 for k- epsilon RNG flow and $\alpha=0.0$ degree

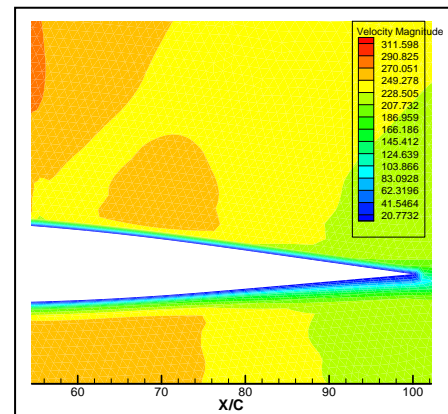


Fig.13a velocity magnitude contours at Mach number 0.7for k- epsilon RNG flow and $\alpha=0.0$ degree

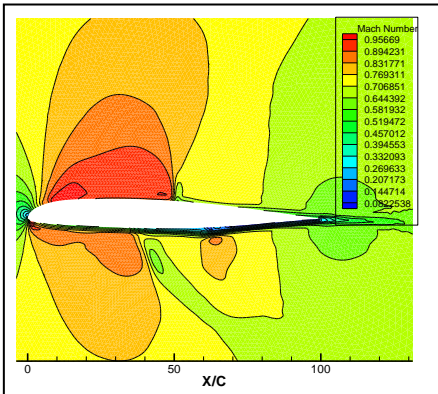


Fig 14 Mach number contours (free stream at Mach number 0.7 for Spalart-Allmaras flow and $\alpha=0.0$

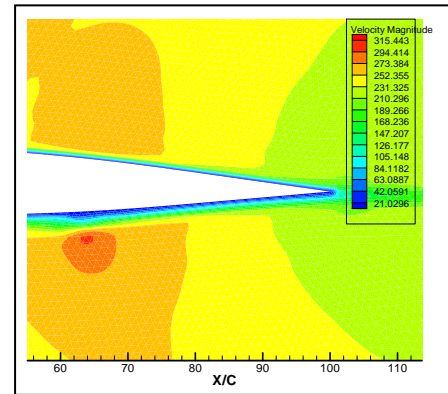


Fig.14a velocity magnitude contours at Mach number 0.7 for Spalart- Allmaras flow and $\alpha=0.0$

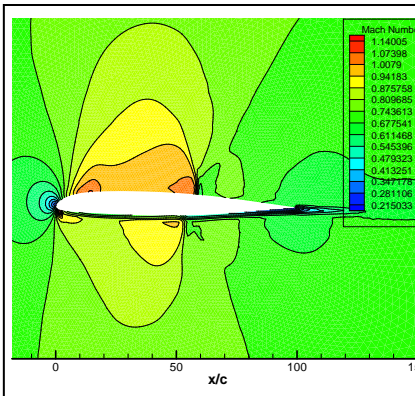


Fig 15 Mach number contours (free stream at Mach number 0.729 for inviscid flow) and $\alpha=0.0$ degree)

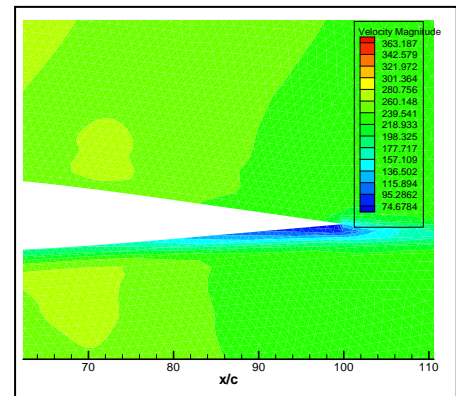


Fig.15a velocity magnitude contours at Mach number 0.729 for inviscid flow and $\alpha=0.0$ degree

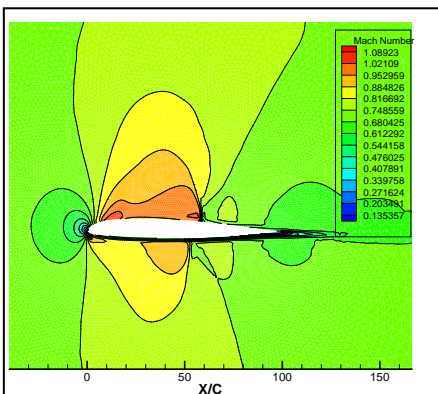


Fig 16 Mach number contours (free stream at Mach number 0.729 for k epsilon RNG flow and $\alpha=0.0$ degree

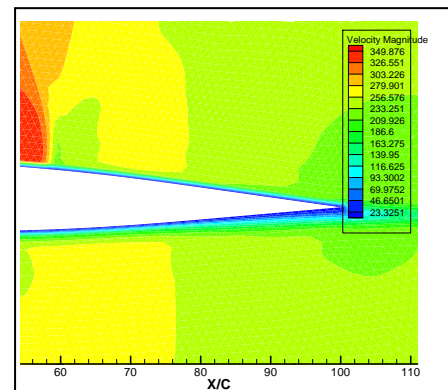


Fig.16a velocity magnitude contours at Mach number 0.729 for k-epsilon RNG flow and $\alpha=0.0$ degree

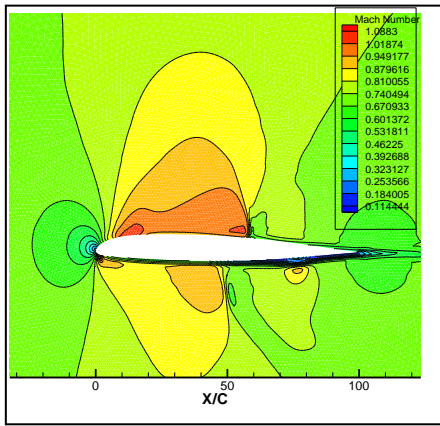


Fig 17 Mach number contours (free stream at Mach number 0.729 for Spalart Allmaras flow and $\alpha=0.0$ degree)

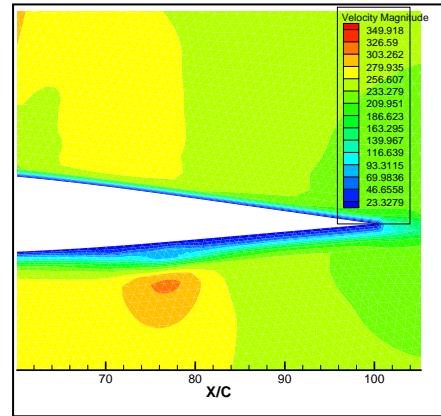


Fig.17a velocity magnitude contours at Mach number 0.729 for Spalart Allmaras flow and $\alpha=0.0$ degree

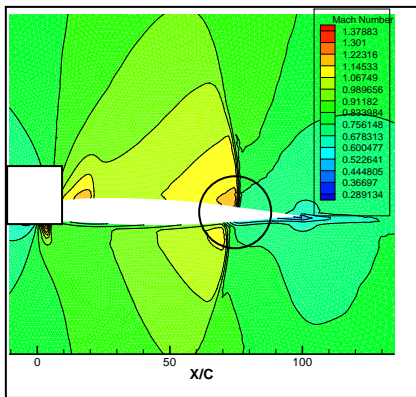


Fig 18 Mach number contours (free stream at Mach number 0.8 for inviscid flow and $\alpha=0.0$ degree)

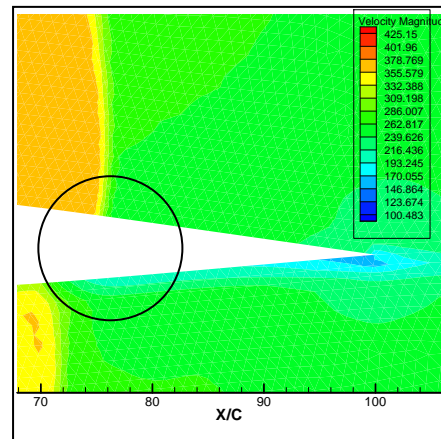


Fig.18a velocity magnitude contours at Mach number 0.8 for inviscid flow and $\alpha=0.0$ degree

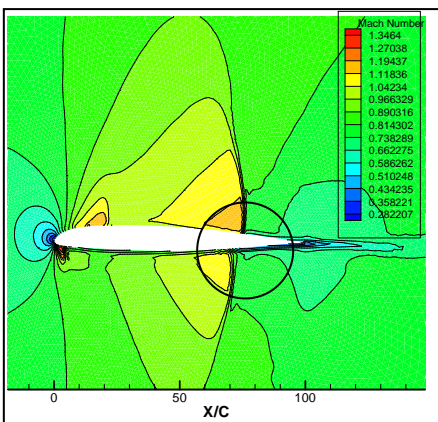


Fig 19 Mach number contours (free stream at Mach number 0.8 for k epsilon RNG flow and $\alpha=0.0$ degree)

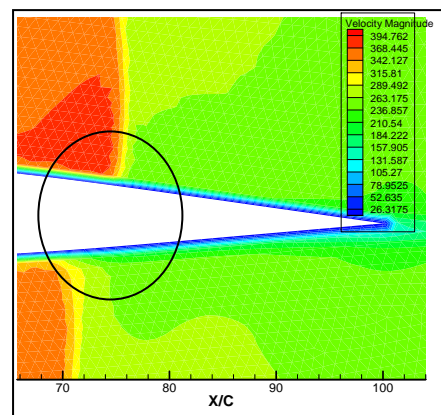


Fig.19a velocity magnitude contours at Mach number 0.8 for k-epsilon RNG flow and $\alpha=0.0$ degree

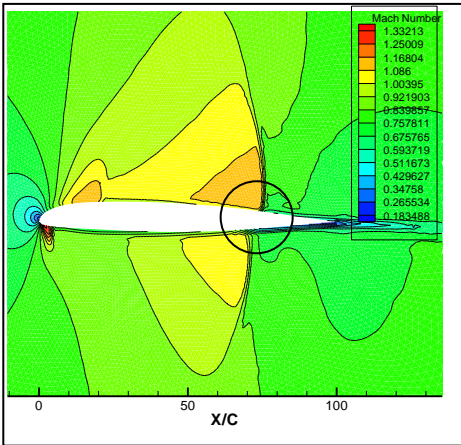


Fig 20 Mach number contours (free stream at Mach number 0.8 for Spalart-Allmaras flow and $\alpha=0.0$ degree)

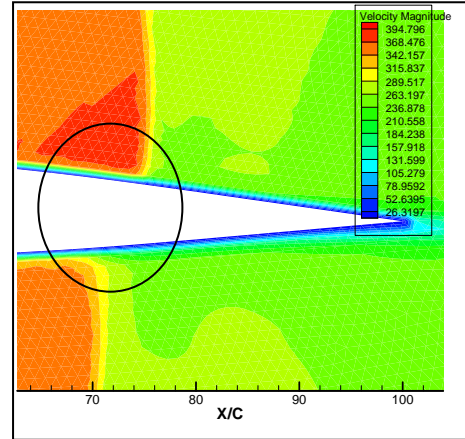


Fig.20a velocity magnitude contours at Mach number 0.8 for Spalart-Allmaras flow and $\alpha=0.0$ degree

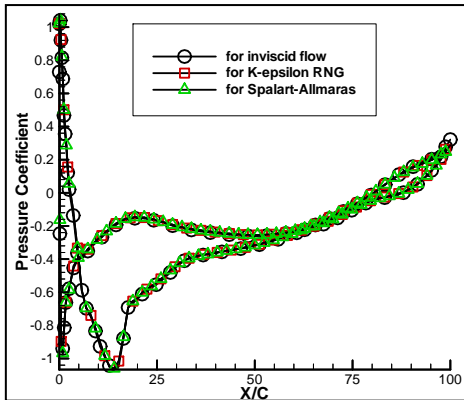


Fig.21 Comparison of Pressure Coefficient Distribution (Free stream Mach number 0.7)

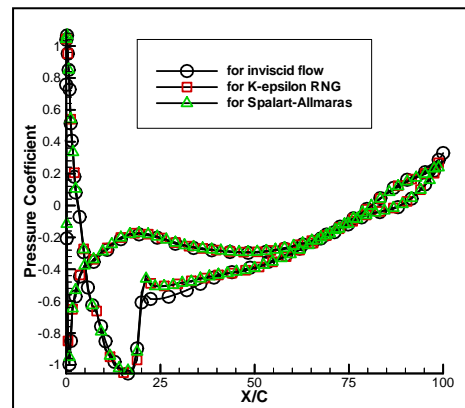


Fig.22 Comparison of Pressure Coefficient Distribution (Free stream Mach number 0.729)

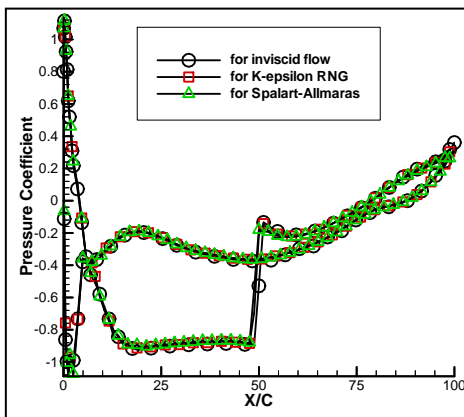


Fig23 Comparison of Pressure Coefficient Distribution (Free stream Mach number 0.8)

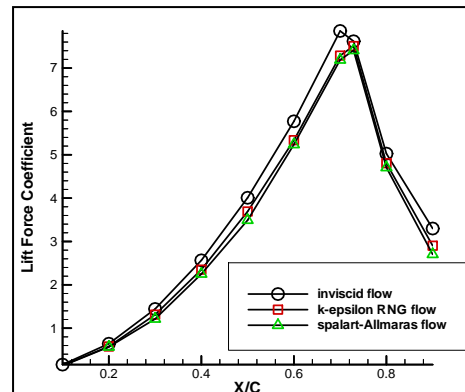


Fig 24Lift force coefficient (C_L) at Mach numbers from (0.1 to 0.9) for inviscid and viscose flow

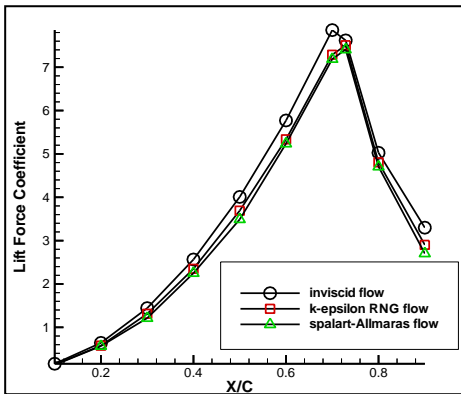


Fig.25 Drag force coefficient (C_D) at Mach numbers from (0.1 to 0.9) for inviscid and viscose flow

References

1. Omar Badran, Regis Quadros and Fettah Aldudak *“Two-Equation Turbulence Models for Turbulent Flow over a NACA 4412 Airfoil at Angle of Attack 15 Degree”* Mechanical Engineering Department Faculty of Engineering technology, Al-Balqa` Applied University, P.O.Box 331006, Amman 11134 – Jordan (2003)
2. Serhat Duran *“Computer-Aided Design Of Horizontal-Axis Wind Turbine Blades ”* Partial Fulfillment of the requirements for the Degree of Master of Science in Mechanical Engineering, Middle East Technical University (2005).
3. B. Greschner, C. Yu, S. Zheng, M. Zhuang, Z. J. Wang and F. Thiele* *“Knowledge Based Airfoil Aerodynamic and Aeroacoustic”* Hermann-Foettinger-Institute of Fluid Mechanics Berlin University of Technology, Mueller-Breslau-Str. 8, D-10623 Berlin, Germany(2005).
4. Manish K. Singh, K. Dhanalakshmi and S. K. Chakrabarty *“ Navier-Stokes Analysis of Airfoils with Gurney Flap”* Computational and Theoretical Fluid Dynamics Division National Aerospace Laboratories P. B. 1779, Bangalore 560 017, India(2005).
5. Ali Al-Hussaini.: *“Computational Study of Supersonic Flow Over Aerodynamic Configurations”* Department of Mechanical Engineering of the University of Technology,(2006).
6. V. Yakhot and S. A. Orszag. *Renormalization Group Analysis of Turbulence: I. Basic Theory.* Journal of Scientific Computing,1(1):1{51, 1986.
7. D. Choudhury. Introduction to the *Renormalization Group Method and Turbulence Modelling Fluent Inc.* Technical memorandum TM-107, 1993
8. S. Sakar and L. Balakrishhnan. *Application of a Reynolds stress Turbulence Model to the Compressible shear layer* ICASE Report 90-18, NASA CR 182002,1990.
9. Chen H. C. and V. C. Patel. *Near-Wall Turbulence Models for Complex Flows Including Separation.* AIAA Journal,26(6):641{648, 1988.
10. *“Fluent Users Services Center”*,2002, WWW.fluentusers.com.
11. Al-Dulaimy, F. M. A.; Cousin, R. *A CFD assessment to transonic flow around a 2822 airfoil* Research Reports from Guest Scientists in the Faculties 07 and 09 in the Academic Year 2004/2005